Multiple scattering of polarized light: Influence of absorption

A Hohmann[1,2], F Voit[1,2], J Schäfer[1] and A Kienle[1]

[1] Institut für Lasertechnologien in der Medizin und Meßtechnik an der Universität Ulm
Helmholtzstr. 12, D-89081 Ulm, Germany

E-mail: alwin.kienle@ilm.uni-ulm.de

Abstract. This work extends a previous contribution about multiple scattering of polarized light propagation in turbid media putting emphasis on the imaginary part of the scatterers' complex refractive index. The whole angle-dependent Müller matrix is evaluated by comparing results of a polarization sensitive radiative transfer solution to Maxwell theory. Turbid media of defined scatterer concentrations are modeled in three dimensions by sphere ensembles kept inside a cubic or spherical simulation volume. This study addresses the impact of absorption on polarization characteristics for selected media from low to high absorption. Besides that, effects caused by multiple and dependent scattering are shown for increasing volume concentration. In this context some unique properties associated with multiple scattering and absorption are pointed out. Further, scattering results in two dimensions are compared for examples of infinite parallel cylinders of high absorption and perpendicularly incident plane waves.

PACS numbers: 42.25.Dd, 42.25.Ja, 87.10.Rt, 95.30.Jx

Keywords: Monte Carlo, radiative transfer, Maxwell theory, polarization, multiple scattering, absorption

[2] A. Hohmann and F. Voit contributed equally to this work.

1. Introduction

An increasing field of biomedical research is dealing with propagation of polarized light in turbid media (Ghosh and Vitkin 2011, Tuchin et al. 2006). While measurement of unpolarized intensity signals already reveals lots of important information about optical properties and conditions of scattering media (Jacques 2013), their assessment can be greatly improved and extended by inclusion of polarization. Many applications in medical diagnostics are profiting from polarization properties, e.g. noninvasive glucose sensing, tissue anisotropy or concentration measurements, amongst others (Tuchin et al. 2006).

For assignment of these experimental data to theory, various light propagation simulation models based on different grades of accuracy have been developed in recent years. An emerging number of them is also taking into account polarization (Akarçay and Ricka 2011, Doronin et al. 2014). In a macroscopic point of view, determination of the far-field Müller matrix yields sufficient polarization properties of the scattering system for most applications. High demands in accuracy are vital to validate these state-of-the-art simulation methods with respect to the whole Müller matrix (Ghosh and Vitkin 2011).

Regarding the physical framework of scattering simulations, radiative transfer theory and its numerical solutions (especially Monte Carlo models) show a high level of practical relevance as scattering problems in extended simulation volumes can be handled. Moreover, statistical models like Monte Carlo techniques bring out accurate results, often superior to spatially discretized numerical solution methods of the radiative transfer equation, in a reasonable amount of time. In recent times some research was conducted (Kuzmin and Meglinski 2006, Meglinski and Kuzmin 2011, Kuzmin and Meglinski 2007) by development of Monte Carlo models which even consider coherent effects. Nevertheless since common radiative transfer models in biophotonics often don't consider these coherent effects, their solutions are approximative, taking into account mostly an intensity-based angular phase function. This is a possible source of error and was investigated in the present study. A more precise wave optics approach considering coherent effects (cf. 3.3) is given by Maxwell theory even though its solutions require extensive amounts of computational power. However, depending on complexity of the modeled media, there are some conditions under which analytical solutions of Maxwell's equations are known. For instance, many models for isotropic turbid media are based on mono- and polydisperse spherical scatterers of defined size distributions and optical properties. These simplified models can also be used to model biological materials (Schneiderheinze et al. 2007).

In publications dealing with primarily isotropic samples the properties of scattering cross sections were shown in case of unpolarized light when radiative transfer theory and Maxwell theory are compared in two or three dimensions (Schäfer and Kienle 2008, Voit et al. 2009). The results indicate that the Monte Carlo method can be applied to media of considerable scatterer concentrations where good agreement can be achieved. Similar results were retrieved for a new polarization sensititve Monte Carlo approach when all angularly resolved Müller matrix elements are compared to Maxwell theory (Voit et al. 2012). The angular shape of each Müller matrix element showed characteristic effects due to dependent and multiple scattering. However, the scattering was only calculated for non-absorbing particles in these studies, thus limiting the applicability of the results.

The aim of this study is to illustrate differences and similarities in the propagation

of polarized light through scattering and absorbing particles ($\mathrm{Im}(n) > 0$) calculated by radiative transfer in comparison to Maxwell theory. The normalized angular results of all independent Müller matrix elements are compared for increasing concentrations and for different absorptions of the scatterers. Further, models made of parallel infinite cylinders, where the propagation of perpendicularly incident light is restricted to two dimensions, are compared complementary to the three-dimensional case of spheres for interpretation of the results.

2. Methods

Two solution paths for calculating polarized light propagation in turbid media including absorbing scatterers are compared in this investigation:

- as numerical solution of the radiative transfer theory a polarized Monte Carlo (MC) code was implemented,
- as analytical reference solutions of Maxwell theory the Generalized Multisphere Mie method GMM (Xu 1995) and the multiple cylinder code in MatScat (Schäfer 2012) were used for three- and two-dimensional cases, respectively.

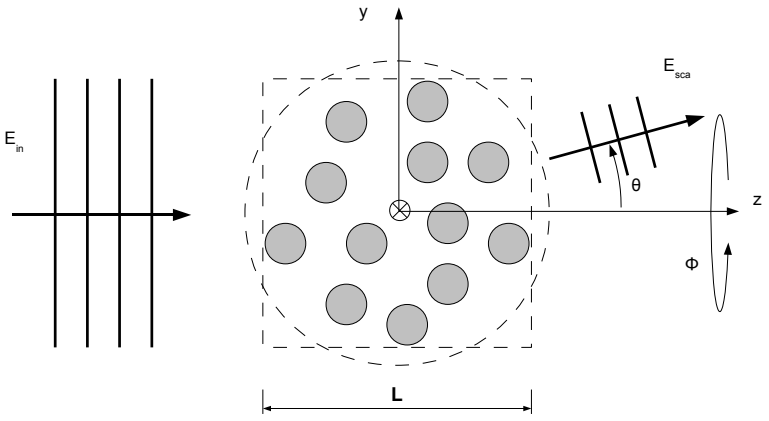

Figure 1. Schematic model for multisphere scattering. Monochromatic light incident in +z direction is multiply scattered by absorbing and scattering spheres, restricted to a cubical (or spherical) simulation volume, and registered for all angular directions θ and ϕ.

In Fig. 1 the investigated scattering scene is depicted which both methods are based on. Different collections of spherical scatterers ($N = 12, 24, 48$ and 96) of radius $r = 1$ μm were randomly generated in a cubic simulation volume of edge length $L = 10$ μm corresponding to volume concentrations $f_V = 5.03$ vol%, 10.05 vol%, 20.11 vol% and 40.21 vol%, respectively. Note that to be consistent with our previous investigation (Voit et al. 2012) the volume concentrations and size parameters were kept. However, in this investigation the scattering spheres also feature absorbing characteristics, specified by different complex refractive indices ($n_s = 1.59 + 0.00$i, $1.59 + 0.01$i, $1.59 + 0.10$i and $1.59 + 1.00$i). In all further occurrances within this article the imaginary part of the complex index of refraction $\mathrm{Im}(n)$ will be abbreviated as 'absorption index' and should not be confused with other definitions. As illustrated in

Table 1. Selected test cases simulated using the Maxwell solution as well as the Monte Carlo method. The absorption and scattering coefficients μ_a and μ_s result from the different volume concentrations f_V and refractive indices n_s. Both were calculated assuming the single sphere Mie solution and used as input for the Monte Carlo program.

Case	# Spheres	f_V [vol%]	n_s	$\mu_a[\mathrm{mm}^{-1}]$	$\mu_s[\mathrm{mm}^{-1}]$
1.1	12	5.03	$1.59 + 0.00\mathrm{i}$	0	111.73
1.2	12	5.03	$1.59 + 0.01\mathrm{i}$	12.39	96.18
1.3	12	5.03	$1.59 + 0.10\mathrm{i}$	42.34	49.25
1.4	12	5.03	$1.59 + 1.00\mathrm{i}$	38.62	47.63
2.1	24	10.05	$1.59 + 0.00\mathrm{i}$	0	223.46
2.2	24	10.05	$1.59 + 0.01\mathrm{i}$	24.77	192.36
2.3	24	10.05	$1.59 + 0.10\mathrm{i}$	84.67	98.50
2.4	24	10.05	$1.59 + 1.00\mathrm{i}$	77.24	95.26
3.1	48	20.11	$1.59 + 0.00\mathrm{i}$	0	446.91
3.2	48	20.11	$1.59 + 0.01\mathrm{i}$	49.54	384.72
3.3	48	20.11	$1.59 + 0.10\mathrm{i}$	169.34	196.99
3.4	48	20.11	$1.59 + 1.00\mathrm{i}$	154.47	190.52
4.1	96	40.21	$1.59 + 0.00\mathrm{i}$	0	893.82
4.2	96	40.21	$1.59 + 0.01\mathrm{i}$	99.09	769.43
4.3	96	40.21	$1.59 + 0.10\mathrm{i}$	338.68	393.98
4.4	96	40.21	$1.59 + 1.00\mathrm{i}$	308.94	381.04

2.1 the absorption coefficient of the sample can be calculated from the spheres' cross sections and volume concentrations. An overview of the parameters used for all test cases is given in Table 1, where the refractive index of the host medium embedding the spheres was set to $n_m = 1.33$. The size of the spherical scatterers has been chosen as tradeoff between providing access to the multiple scattering regime and minimizing the number of scatterers. The drawback are more oscillations by the phase function of an individual scatterer rendering the interpretation of the results more sophisticated.

The scattering is subject to the following assumptions. A plane monochromatic wave ($\lambda = 600$ nm) irradiates the simulation volume perpendicularly to one side, then its scattered light is registered in the far-field for each scattering angle θ and azimuthal angle ϕ. The results, averaged over all azimuthal angles ϕ for both methods in order to suppress statistical noise and interference speckles, are converted to the scattering Müller matrix of the whole system to point out the polarization-dependent scattering characteristics. Each matrix element is normalized (apart from the first) to the unpolarized intensity and evaluated for the total range of scattering angles θ from 0 to 180 degrees. Details about both simulation methods and the referring Müller matrix formalism are illustrated in literature (Bohren and Huffman 1998, Voit et al. 2012) and are applied here in an analogous way. In further simulations the impact of the boundary shape of the simulation volume to the scattering function was investigated. Therefore a spherical boundary (see Fig. 1) of the sphere collection was programmed to explore the shape influence of the surface at which the incident wave hits the simulation volume. For this case a random sequential addition algorithm was used to generate multiple realizations of random scatterer arrangements within a sphere without overlap.

2.1. Monte Carlo method

The principle of the first method, a Monte Carlo solution of the radiative transfer theory, can be found in literature (Bartel and Hielscher 2000, Raković et al. 1999, Côté and Vitkin 2005, Kattawar and Adams 1989, Maksimova et al. 2002, Ramella-Roman et al. 2005, Wang and Wang 2002, Voit et al. 2012) and is briefly sketched in this section. In general, many propagation paths of light 'photons' through a scattering medium are calculated. The photons enter the simulation volume at one side and are once or multiply scattered before being detected when they exit the volume. The corresponding exit angles are registered and summed up for every direction to get a statistical intensity distribution in the far-field. Inside the scattering volume each scattering event is characterized by a random choice of scattering length and direction which obey the Beer-Lambert law and the single sphere Mie (Bohren and Huffman 1998) phase function, respectively. The scattering coefficients μ_s and absorption coefficients μ_a are needed for the Monte Carlo program to specify the extinction lengths of the stochastic process. They are calculated via the Mie formalism as well and depend on the number fraction N/V of the spheres and their scattering and extinction cross sections C_{sca} and C_{ext} according to $\mu_s = N/V \cdot C_{sca} = f_V/V_s \cdot Q_{sca} \cdot \pi \cdot r^2 = 3 \cdot f_V \cdot Q_{sca}/(4 \cdot r)$ and $\mu_a = N/V \cdot (C_{ext} - C_{sca}) = 3 \cdot f_V \cdot (Q_{ext} - Q_{sca})/(4 \cdot r)$ using the volume of a single sphere V_s, the volume fraction f_V of N spheres in a volume V and the efficiencies defined by $Q = C/(\pi \cdot r^2)$. Here the absorption values are indirectly retrieved as the difference of extinction and scattering values. To determine the polarization properties of the total simulation volume the angularly resolved Müller matrix is obtained by subsequent simulation of four different incident Stokes vectors $(I_i, Q_i, U_i, V_i)^T$ scattered by the whole system. The Müller matrix of a single scattering event can be directly pieced together using the Mie solution:

$$\begin{pmatrix} I_s \\ Q_s \\ U_s \\ V_s \end{pmatrix} = \frac{1}{k^2 r^2} \begin{pmatrix} S_{11} & S_{12} & 0 & 0 \\ S_{12} & S_{11} & 0 & 0 \\ 0 & 0 & S_{33} & S_{34} \\ 0 & 0 & -S_{34} & S_{33} \end{pmatrix} \begin{pmatrix} I_i \\ Q_i \\ U_i \\ V_i \end{pmatrix} . \tag{1}$$

For every scattering event the coordinate system of the Stokes vector is transformed to the scattering plane. After the Stokes vector was changed by application of the Müller matrix, the coordinate system was back transformed to the global coordinate system, again for each scattering event (Bartel and Hielscher 2000, Ramella-Roman 2005, Rakovic 1999).

Hence four scattered (polarized) Stokes vectors $(I_s, Q_s, U_s, V_s)^T$ build the scattering Müller matrix which describes the polarization impact of the whole system after multiple scattering events. According to the applied incident Stokes vectors $(1,1,0,0)^T$, $(1,-1,0,0)^T$, $(1,0,1,0)^T$ and $(1,0,0,1)^T$, labeled here as H, V, P and R (Hielscher et al. 1997), the components of the four corresponding scattered Stokes vectors, averaged over multiple photon paths, can be employed and the Müller matrix can be written in the form (Tuchin et al. 2006):

$$M = \frac{1}{2} \begin{pmatrix} I_H + I_V & I_H - I_V & 2I_P - I_H - I_V & 2I_R - I_H - I_V \\ Q_H + Q_V & Q_H - Q_V & 2Q_P - Q_H - Q_V & 2Q_R - Q_H - Q_V \\ U_H + U_V & U_H - U_V & 2U_P - U_H - U_V & 2U_R - U_H - U_V \\ V_H + V_V & V_H - V_V & 2V_P - V_H - V_V & 2V_R - V_H - V_V \end{pmatrix} . \tag{2}$$

2.2. Maxwell solution

The second method for calculation of the angularly resolved Müller matrix is the solution of Maxwell theory. For three-dimensional simulations of multiple sphere systems the Generalized Multisphere Mie method GMM (Xu 1995) has been used which provides analytical solutions in form of the angle-dependent scattering Müller matrix in case of an incident plane wave. As a solution of Maxwell theory the exact boundary value problem must be solved which requires knowledge of the spheres' refractive indices, radii and positions (without overlap). For each case listed in Table 1 10 different randomly generated spatial distributions of the spheres within the medium were simulated and the results were ensemble-averaged for an acceptable reduction of the interference speckles. More details of this method are described in literature (Voit et al. 2012). Contrary to the statistical Monte Carlo technique, where the volume concentration and extinction cross section of the turbid medium are both contained in the extinction coefficient, the GMM method requires a specific number of spherical scatterers exhibiting complex refractive indices.

An important aspect of this publication consists in the inclusion of the absorption property of the scatterers. This renders the scatterer model more realistic for many biomedical applications. For example, human tissue can incorporate particulate matter of high absorption like soot or pyroclastic microparticles (Horwell 2007, Ling et al. 2011, Hull and Abraham 2002). To specify the meaning of absorption regarding cellular scatterers in Mie size regime some remarks have to be made. First, absorption is included in the complex refractive index of the scatterers. For the host medium, the imaginary part of the refractive index and thus the absorption was set to zero. An exact model based on multiple scattering in absorptive host media is difficult to interpret for far-field measurements because the scattered intensity is not only angularly dependent but also sensititve to distances between scatterers and light source as well as detector. Further, application of such a model would be appropriate in cases where light only survives few scattering events. However, the zero-absorption host medium approximation is valid for many cases in biomedical optics since most extracellular media are primarily made of water having quite low absorption indices in the visible wavelength range. A word of caution about the choice of complex refractive indices of the scatterers must be added. Though the absorption cross section is often noted to be proportional to the refractive index' imaginary part, this only holds for wave propagation in homogeneous media. On the other hand, Mie theory leads to a non-monotonic behaviour of the absorption where cross sections depend on the scatterer size as well as the complex refractive index of the scatterers. Thus, increasing the imaginary part of the scatterer refractive index has additional impact on the scattering coefficient. For very high imaginary parts the contribution of scattering even outperforms that of absorption, so that for Mie scatterers absorption cross sections decrease after hitting a maximum, mostly at $\mathrm{Im}(n) \lesssim 0.2$ for the size parameters under consideration. The used values of the scatterers' refractive indices are arbitrarily chosen to simulate scattering of polystyrol spheres and absorption in different orders of magnitude. This serves as a basis for many standard assemblies and test models in biomedical optics (Hull et al. 1998, Ma et al. 2003).

2.3. Quantitative comparison

Figs. 2-9 show the normalized form of the angularly resolved Müller matrix. All elements except the first were normalized to M_{11} for each scattering angle θ. The M_{11} element itself was normalized to the forward direction of the Monte Carlo solution to improve illustration. Exactly the same normalization factor was applied to the results of the Maxwell solution as well as of the Monte Carlo solution. Therefore, it was possible to directly compare the calculated scattering characteristics of both solution approaches for the whole scattering angle range.

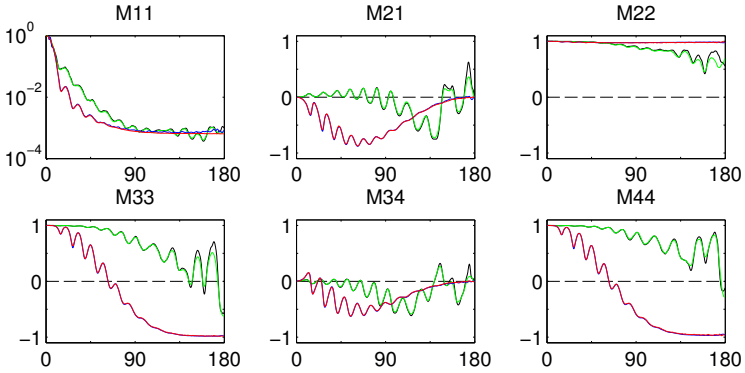

Figure 2. Independent Müller matrix elements for $N = 12$ spheres ($f_V = 5.03$ vol%). Every normalized element is plotted against the scattering angle θ. Maxwell and Monte Carlo results for $n_s = 1.59 + 0.00\mathrm{i}$ are illustrated as black and green curves, for $n_s = 1.59 + 1.00\mathrm{i}$ as blue and red curves, respectively.

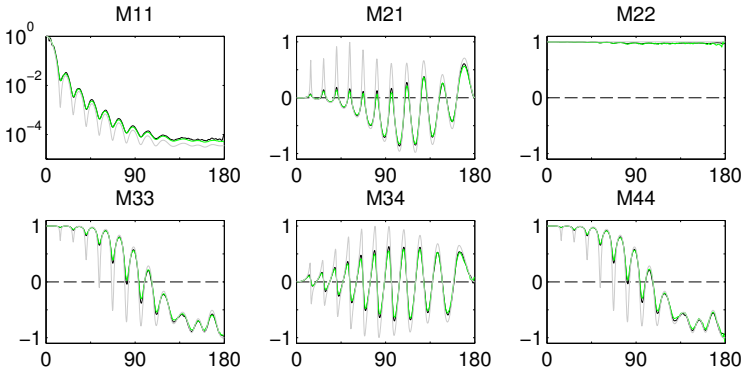

Figure 3. Independent Müller matrix elements for $N = 12$ spheres ($f_V = 5.03$ vol%). Every normalized element is plotted against the scattering angle θ. Maxwell and Monte Carlo results are illustrated as black and green curves for $n_s = 1.59 + 0.10\mathrm{i}$. The normalized Mie solution of an individual sphere (grey curve) is included for comparison.

For randomly distributed ensembles of spherical scatterers the Müller matrix has a particular symmetry, i.e. not all 16 elements are independent from each other. Some

research has been conducted in this field since the introduction of the Müller calculus and was verified for spatially as well as angularly resolved measurements (Hovenier et al. 2003, Van de Hulst 1981). In case of mirror-symmetric, macroscopically isotropic ensembles (Mishchenko et al. 2006) the Müller matrix occupies a block-diagonal shape of 6 independent elements, cf. Eq. (1), in detail M_{11}, M_{21}, M_{22}, M_{33}, M_{34} and M_{44}, where $M_{12} = M_{21}$ and $M_{43} = -M_{34}$, all further elements vanish.

Simulations of light propagation in two dimensions are based on random ensembles of parallel infinite circular cylinders and perpendicularly incident light. The Matlab framework Matscat (Schäfer 2012) provides an analytical multiple cylinder code which is based on the algorithm by Lee (Lee 1990). Since the propagation directions of the scattered light are all contained in one scattering plane perpendicular to the cylinder axes the light scatter is restricted to two dimensions.

3. Results and discussion

For four different volume concentrations f_V and absorption indices $\mathrm{Im}(n)$ of the scatterers all 16 angularly resolved Müller matrix elements were calculated using both the Monte Carlo and the GMM method.

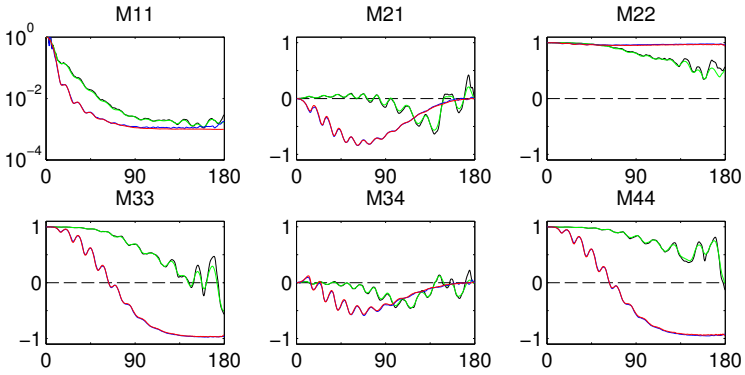

Figure 4. Same as Fig. 2, but for $N = 24$ spheres ($f_V = 10.05$ vol%).

The block-diagonal shape and symmetry of the Müller matrix was reproduced for all simulation cases. Only the relevant independent elements M_{11}, M_{21}, M_{22}, M_{33}, M_{34} and M_{44} are depicted in Figs. 2-9 for every investigated simulation case. Each figure contains the results of the Monte Carlo simulations as well as of the Maxwell solutions. There were a number of interesting effects and characteristic features which are pointed out and evaluated in the subsequent sections.

3.1. Dependency on refractive index

The results for $n_s = 1.59 + 0.01\mathrm{i}$ show almost the same behaviour as the results for $n_s = 1.59 + 0.00\mathrm{i}$ (Figs. 2, 4, 6, and 8) for all concentrations and Müller matrix elements and are not explicitly shown. Only the intensity values (M_{11} element) for $n_s = 1.59 + 0.00\mathrm{i}$ clearly exceed the values for $n_s = 1.59 + 0.01\mathrm{i}$ for all angles except $\theta = 0$. This can be explained by the existing absorption for $n_s = 1.59 + 0.01\mathrm{i}$ (see

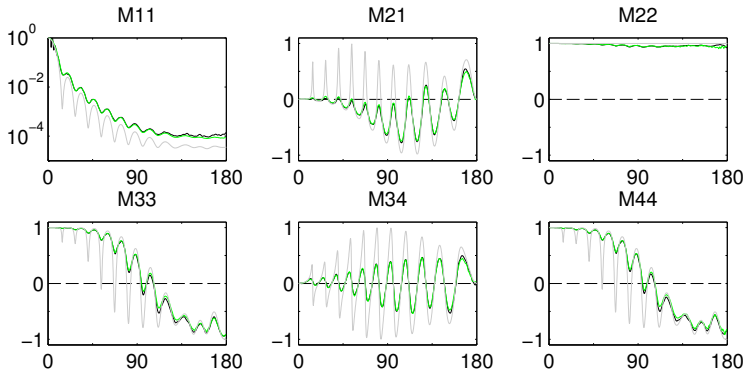

Figure 5. Same as Fig. 3, but for $N = 24$ spheres ($f_V = 10.05$ vol%).

Table 1) which leads to a non-negligible loss of light intensity within the simulation volume.

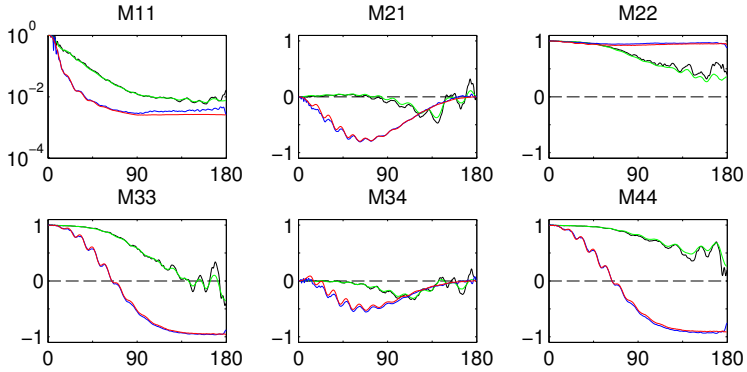

Figure 6. Same as Fig. 2, but for $N = 48$ spheres ($f_V = 20.11$ vol%).

Large variations in the Müller matrix elements can be observed between different refractive indices. A strong dependence on the scattering angle is visible for $n_s = 1.59 + 0.00\mathrm{i}$ (Figs. 2, 4, 6, and 8) and especially for $n_s = 1.59 + 0.10\mathrm{i}$, where large oscillations are present over the whole angular range (Figs. 3, 5, 7, and 9). These large oscillations result from the Mie solution of an individual sphere which also shows a similar pattern for $n_s = 1.59 + 0.10\mathrm{i}$ and is added normalized to these figures for comparison.

We note that the oscillations disappear for $n_s = 1.59 + 1.00\mathrm{i}$ especially in the backscattering region, where the Müller matrix approximates the properties of a half-wave plate. That means, that the matrix approaches a diagonal matrix with $M_{22} = 1$, $M_{33} = -1$ and $M_{44} = -1$ for angles near 180 degrees. The oscillations are better conserved for small scattering angles even for a refractive index of $n_s = 1.59 + 1.00\mathrm{i}$. The afore-mentioned oscillations show a rather complex pattern of the Müller matrix elements strongly depending on the scattering angle.

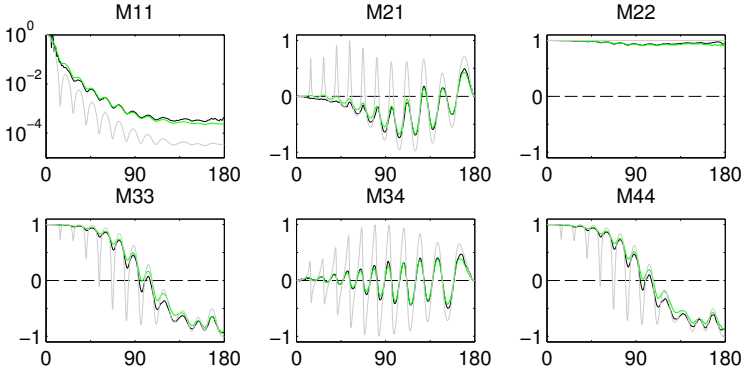

Figure 7. Same as Fig. 3, but for $N = 48$ spheres ($f_V = 20.11$ vol%).

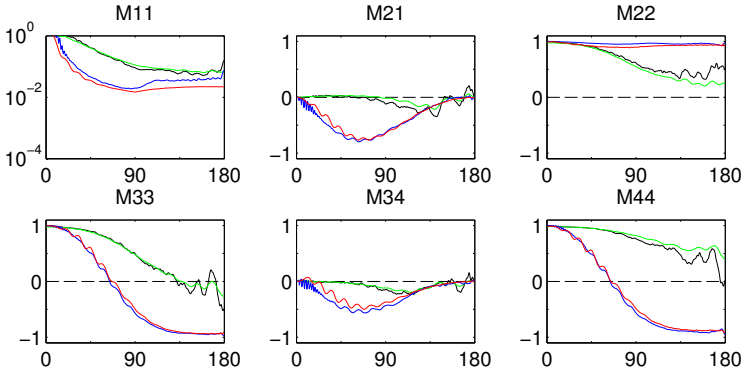

Figure 8. Same as Fig. 2, but for $N = 96$ spheres ($f_V = 40.21$ vol%).

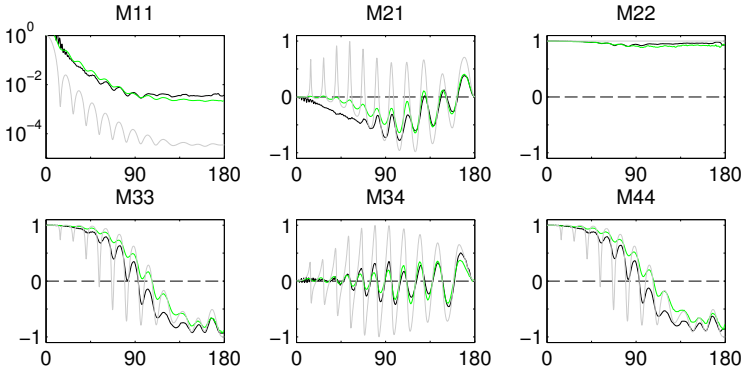

Figure 9. Same as Fig. 3, but for $N = 96$ spheres ($f_V = 40.21$ vol%).

For several Müller matrix elements some minor differences between the Monte Carlo simulations and the Maxwell solution are visible for $n_s = 1.59 + 0.00\mathrm{i}$ in the backscattering region, even for small concentrations. These differences become smaller for higher absorption indices for all elements except the M_{11} element.

A further effect visible for higher refractive indices is that the M_{22} element approaches the value of 1 for all scattering angles, which is a sign for predominant single scattering. The M_{33} element approaches the M_{44} element which is a further affirmation for single scattering being predominant. Besides that, it can be observed, that these elements decrease with increasing absorption index. For $n_s = 1.59 + 0.00\mathrm{i}$, the absolute values of all normalized matrix elements except M_{11} generally decrease at higher scattering angles for higher volume concentrations, which points towards multiple scattering (Tuchin et al. 2006). This effect is not as prominent for high absorption indices, which is a further indicator for prevalent single scattering in case of high absorptions.

An interesting peculiarity can be observed for scattering angles $\theta \geq 90\,\mathrm{deg}$ in case of a higher absorption index. The Maxwell solution of the M_{11} element of the Müller matrix strongly deviates from the Monte Carlo solution in this angular range. An increasing imaginary part of the refractive index of the scattering spheres showed increasing differences for the M_{11} element. This effect becomes more pronounced if high scatterer concentrations are taken into account and is not visible for the refractive indices $n_s = 1.59 + 0.00\mathrm{i}$ or $n_s = 1.59 + 0.01\mathrm{i}$.

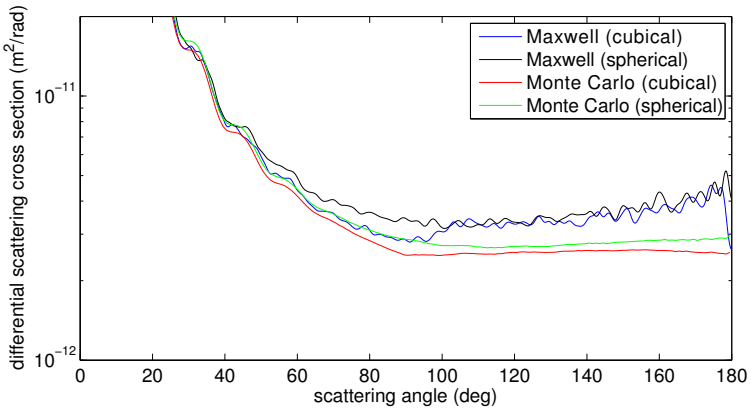

Figure 10. Differential scattering cross section versus scattering angle θ for $N = 48$ spheres ($f_V = 20.11$ vol%) and $n_s = 1.59 + 1.00\mathrm{i}$, showing the shape influence of the simulation volume. To keep the volume concentration constant for a certain number of spheres, the diameter of the bounding sphere has been set to 12.407 μm (in comparison to the edge length $L = 10$ μm for the cube).

This behaviour conincides with an increase of the intensity element M_{11} for scattering angles $\theta \geq 90\,\mathrm{deg}$ for both solution methods, which is more pronounced for the Maxwell solution. This increase is attributed to the geometrical shape of the simulation volume. Fig. 10 shows the M_{11} element for a cubical simulation volume having a volume concentration of $f_V = 20.11$ vol% as well as a corresponding simulation with a sphere as simulation volume. This spherical simulation volume (diameter 12.407 μm) was filled with the same number of scattering spheres as the

cubical simulation volume ($L = 10$ μm) such that the same volume concentration was reached. It is obvious, that the abrupt increase of the M_{11} element at $\theta \geq 90$ deg disappears for the spherical simulation volume for the Maxwell solution as well as for the Monte Carlo solution. The same behaviour was also observed for the higher volume concentration of $f_V = 30.16$ vol% (data not shown) which the random sequential addition algorithm was still able to model. This increase of the M_{11} element for $\theta \geq 90$ deg could point towards near-surface scattering, being clearly prominent for the plane surface of the cubical simulation volume, where the wave is incident, and being smoothed out for the curved surface of the spherical simulation volume.

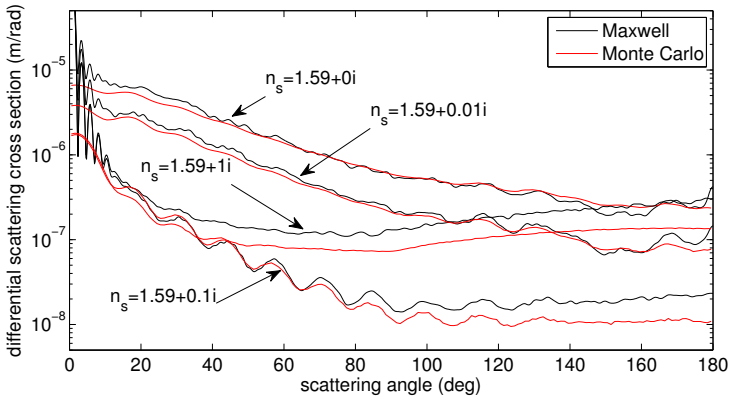

Figure 11. Differential scattering cross sections for $N = 13$ infinite parallel cylinders ($f_V = 40.84$ vol%) for perpendicularly incident light, plotted against the scattering angle θ. The quadratic bounding box of the cylinder distribution has an edge length of $L = 10$ μm. Unpolarized Maxwell (black) and Monte Carlo results (red) are shown pairwise for different absorption indices.

Furthermore, it was investigated, if the distinct increase for scattering angles $\theta \geq 90$ deg also occurs in two dimensions. The solution of a plane wave ($\lambda = 600$ nm) incident on an assembly of $N = 13$ infinitely extended scattering cylinders of radius $r = 1$ μm, randomly distributed in a quadratic bounding box of edge length $L = 10$ μm, showed similar results as previously described for spheres. Fig. 11 shows the angularly resolved differential scattering cross section averaged over 1000 random ensembles for refractive indices of $n_s = 1.59+0.00$i, $n_s = 1.59+0.01$i, $n_s = 1.59+0.10$i and $n_s = 1.59 + 1.00$i, respectively. If these curves are compared to the respective M_{11} elements in the three-dimensional case (Figs. 8 and 9), a comparable behaviour of the results was observed which confirms the abrupt increase for scattering angles $\theta \geq 90$ deg in two dimensions as well, although not as steep. As in the multisphere case the Maxwell solution shows values above those of the Monte Carlo solution for almost the whole angular range and for high absorption indices ($n_s = 1.59 + 1.00$i). Besides that the separation between the intensity results for higher volume concentrations due to dependent scattering (cf. section 3.3) appears to begin at rather small scattering angles compared to the three-dimensional case.

3.2. Dependency on volume concentration

The results indicate good agreement of the overall shape of the Müller matrix elements especially for small scatterer concentrations. This agreement was already observed for unpolarized and polarized light without absorption (Voit et al. 2012) and was now observed for absorbing scatterers within this study (Hohmann et al. 2012). However, there are increasing deviations between the two methods for increasing scatterer concentrations, most prominent for higher scattering angles. As multiple scattering is considered by both solution methods, these differences are supposed to be a dependent scattering effect. In this study it was found that for large volume concentrations, dependent scattering effects lead to increasing differences between the two solution methods for absorbing scatterers, as it was already described for non-absorbing scatterers (Voit et al. 2012). These differences seem to be most prominent for high scatterer concentrations and high absorptions. They are clearly visible for the concentration $f_V = 40.21$ vol% and $n_s = 1.59 + 0.10\mathrm{i}$ (see Fig. 9), where μ_a has rather high values (see Table 1). For this concentration and refractive index especially the M_{12} element exhibits obvious deviations between the two solution methods for small scattering angles.

The M_{22} element decreases with increasing volume concentration especially in the backward scattering region for small absorptions (e.g. Fig. 8). The deviation from unity is a sign for multiple scattering of the light emitted in backward direction.

The overall shape of the Müller matrix elements remains roughly similar for all concentrations at the same scatterer refractive index. This holds for all investigated indices of refraction. However, more oscillations over the scattering angle can be observed in case of small concentrations for all indices of refraction. These oscillations result from the single Mie solution and decrease with increasing scatterer concentrations. The flattening effect is mainly attributed to multiple scattering and is visible for both solution methods. Nevertheless it can be also seen (e.g. Fig. 9) that even in case of high absorption ($n_s = 1.59 + 0.10\mathrm{i}$), i.e. at lower degree of multiple scattering, the values of all matrix elements flatten in comparison to the single sphere Mie solution for increasing concentrations over the whole angular range.

3.3. Coherent and dependent scattering effects

Large differences between radiative transfer theory and Maxwell theory can be observed especially for the M_{11} element in the low angle range ($\theta \lesssim 10\,\mathrm{deg}$, as illustrated in Fig. 11 for the differential scattering cross section). These deviations are attributed to forward interferences and result from diffraction by the limited simulation volume which the Monte Carlo solution, based on an incoherent phase function, can not handle. This coherent effect is verified for absorbing scatterers similar to the one observed for unpolarized (Voit et al. 2009) and polarized light (Voit et al. 2012) for non-absorbing scatterers. The width of the diffraction peak decreases with increasing size of the simulation volume. Several other Müller matrix elements also exhibit finer oscillations in the scattering region near $\theta = 0\,\mathrm{deg}$ attributed to these forward interferences (e.g. M_{21} and M_{34} in Fig. 8).

Another coherent effect which is preserved for multiple scattering events is coherent backscattering (Mishchenko et al. 2006, Muinonen et al. 2012) leading to a peak of the M_{11} element near 180 degrees which was reproduced by GMM and can in general not be rendered by the common Monte Carlo method. Many more

sphere realizations than simulated within this study would be required for the Maxwell solution to quantify precisely the shape of this peak.

A further source of differences between the exact Maxwell theory and the Monte Carlo results are dependent scattering effects (Brewster and Tien 1982, Göbel et al. 1995, Tishkovets 2008) becoming significant for increasing volume concentrations. Dependent scattering is affected by near-field distortions and spatial scatterer correlations manifesting in far-field interferences which are not included in the Monte Carlo approach. Thus only Maxwell theory as basis of wave optics is able to provide exact coherent solutions.

3.4. Summarized comparison

Good agreement was observed between the Maxwell and the Monte Carlo solutions for all refractive indices and for all Müller matrix elements in case of small concentrations ($f_V \lesssim 10$ vol% in this study, Figs. 2,3,4,5)). Larger differences between the two methods were observed for increasing scatterer concentrations due to dependent scattering. That means, that the radiative transfer theory yields excellent results for small scatterer concentrations even if absorbing scatterers are taken into account. However, the Monte Carlo results have to be treated with care for higher scatterer concentrations. Then, in addition, deviations can occur in case of high absorption indices ($\mathrm{Im}(n) \gtrsim 0.1$ in this study). It was also found, that the differences between the two theories depend not only on the concentration and index of refraction, but also on the polarization properties (variation amongst different Müller matrix elements).

4. Conclusions

The polarized Monte Carlo method is an appropriate radiative transfer theory based method to simulate polarized light propagation in turbid media even if absorbing scatterers are taken into account. It was found that one has to pay attention to possible sources of error if high scatterer concentrations or strongly absorbing particles are to be considered. In this context, the approximative nature of radiative transfer theory to the Maxwell theory becomes visible. Characteristic changes of the Müller matrix elements were observed in cases where the refractive index of the scatterers was varied from $n_s = 1.59 + 0.00\mathrm{i}$ to $n_s = 1.59 + 1.00\mathrm{i}$. Differences between the two solution methods for polarized light propagation in turbid media can be investigated by the presented method for arbitrary particle radii and optical properties of the scatterers.

The results show, in which cases the often used radiative transfer theory is an appropriate approximation to the Maxwell theory and in which cases it deviates significantly. Applications are, amongst further examples, the understanding and optimization of light propagation in tissues in fields like photodynamic therapy, polarization-sensitive and depth-selective tissue investigation or the avoidance of specular reflections when using polarized light. The results of this study can also be used for the interpretation of light propagation in tissues containing incorporated particles of higher absorption. These include for example incorporated soot, metallic, pyroclastic particles or other pigments present in skin tattoos causing typical symptoms like coal worker's pneumoconiosis, smoker's lung and melanoma. After phagocytic encapsulation such particles often reside agglomerated in the tissue in higher concentrations, see e.g. (Ling et al. 2011, Hull and Abraham 2002). Further examples are metallic gold microparticles whose use is also relevant for tumor-

diagnostic and therapeutic purposes (O'Neal et al. 2004). Their impact on polarized light propagation in biological tissues is not fully understood up to now and could be better comprehended using the presented appropriate models.

Acknowledgments

This work was financed by Baden-Württemberg Stiftung gGmbH.

References

Akarçay H and Ricka J 2011 *in* 'Proceedings of SPIE' Vol. 8088 p. 80880K. doi: 10.1117/12.889135.

Bartel S and Hielscher A 2000 Monte Carlo simulations of the diffuse backscattering Mueller matrix for highly scattering media *Applied Optics* **39**(10), 1580–1588. doi: 10.1364/AO.39.001580.

Bohren C and Huffman D 1998 *Absorption and scattering of light by small particles* Wiley-Interscience.

Brewster M and Tien C 1982 Radiative transfer in packed fluidized beds: Dependent versus independent scattering *Journal of Heat transfer* **104**, 573. doi: 10.1115/1.3245170.

Côté D and Vitkin I 2005 Robust concentration determination of optically active molecules in turbid media with validated three-dimensional polarization sensitive Monte Carlo calculations *Optics Express* **13**(1), 148–163. doi: 10.1364/OPEX.13.000148.

Doronin A, Macdonald C and Meglinski I 2014 Propagation of coherent polarized light in turbid highly scattering medium *Journal of Biomedical Optics* **19**(2), 025005–1–025005–8. doi: 10.1117/1.JBO.19.2.025005.

Ghosh N and Vitkin I 2011 Tissue polarimetry: Concepts, challenges, applications, and outlook *Journal of Biomedical Optics* **16**(11), 110801–1–110801–29. doi: 10.1117/1.3652896.

Göbel G, Kuhn J and Fricke J 1995 Dependent scattering effects in latex-sphere suspensions and scattering powders *Waves in random media* **5**(4), 413–426. doi: 10.1088/0959-7174/5/4/003.

Hielscher A, Eick A, Mourant J, Shen D, Freyer J and Bigio I 1997 Diffuse backscattering Mueller matrices of highly scattering media *Optics Express* **1**(13), 441–453. doi: 10.1364/OE.1.000441.

Hohmann A, Voit F, Schäfer J and Kienle A 2012 *in* 'Journal of Physics: Conference Series' Vol. 369 p. 012007. doi: 10.1088/1742-6596/369/1/012007.

Horwell C 2007 Grain-size analysis of volcanic ash for the rapid assessment of respiratory health hazard *Journal of Environmental Monitoring* **9**(10), 1107–1115. doi: 10.1039/B710583P.

Hovenier J, Volten H, Munoz O, Van der Zande W and Waters L 2003 Laboratory studies of scattering matrices for randomly oriented particles: potentials, problems, and perspectives *Journal of Quantitative Spectroscopy and Radiative Transfer* **79**, 741–755. doi: 10.1016/S0022-4073(02)00319-9.

Hull E L, Nichols M G and Foster T H 1998 Quantitative broadband near-infrared spectroscopy of tissue-simulating phantoms containing erythrocytes *Physics in Medicine and Biology* **43**(11), 3381. doi: 10.1088/0031-9155/43/11/014.

Hull M J and Abraham J L 2002 Aluminum welding fume-induced pneumoconiosis *Human pathology* **33**(8), 819–825. doi: 10.1053/hupa.2002.125382.

Jacques S L 2013 Optical properties of biological tissues: a review *Physics in Medicine and Biology* **58**(11), R37. doi: 10.1088/0031-9155/58/11/R37.

Kattawar G and Adams C 1989 Stokes vector calculations of the submarine light field in an atmosphere-ocean with scattering according to a Rayleigh phase matrix: Effect of interface refractive index on radiance and polarization *Limnology and Oceanography* **34**(8), 1453–1472. doi: 10.4319/lo.1989.34.8.1453.

Kuzmin V and Meglinski I 2006 Numerical simulation of coherent backscattering and temporal intensity correlations in random media *Quantum Electronics* **36**(11), 990–1002. doi: 10.1070/QE2006v036n11ABEH013338.

Kuzmin V and Meglinski I 2007 Coherent effects of multiple scattering for scalar and electromagnetic fields: Monte-Carlo simulation and Milne-like solutions *Optics Communications* **273**(2), 307–310. doi: 10.1016/j.optcom.2007.01.025.

Lee S C 1990 Dependent scattering of an obliquely incident plane wave by a collection of parallel cylinders *Journal of applied physics* **68**(10), 4952–4957. doi: 10.1063/1.347080.

Ling S H, McDonough J E, Gosselink J V, Elliott W M, Hayashi S, Hogg J C and Van Eeden S F

2011 Patterns of retention of particulate matter in lung tissues of patients with COPD *Chest* **140**(6), 1540–1549. doi: 10.1378/chest.10-2281.

Ma X, Lu J Q, Brock R S, Jacobs K M, Yang P and Hu X H 2003 Determination of complex refractive index of polystyrene microspheres from 370 to 1610 nm *Physics in Medicine and Biology* **48**(24), 4165. doi: 10.1088/0031-9155/48/24/013.

Maksimova I, Romanov S and Izotova V 2002 The effect of multiple scattering in disperse media on polarization characteristics of scattered light *Optics and Spectroscopy* **92**(6), 915–923. doi: 10.1134/1.1490031.

Meglinski I and Kuzmin V 2011 Coherent backscattering of circularly polarized light from a disperse random medium *Progress In Electromagnetics Research M* **16**, 47–61. doi: 10.2528/PIERM10102106.

Mishchenko M, Travis L and Lacis A 2006 *Multiple scattering of light by particles: Radiative transfer and coherent backscattering* Cambridge Univ. Press.

Muinonen K, Mishchenko M, Dlugach J, Zubko E, Penttilä A and Videen G 2012 Coherent backscattering verified numerically for a finite volume of spherical particles *The Astrophysical Journal* **760**(2), 118. doi: 10.1088/0004-637X/760/2/118.

O'Neal D P, Hirsch L R, Halas N J, Payne J D and West J L 2004 Photo-thermal tumor ablation in mice using near infrared-absorbing nanoparticles *Cancer letters* **209**(2), 171–176. doi: 10.1016/j.canlet.2004.02.004.

Raković M, Kattawar G, Mehrűbeoğlu M, Cameron B, Wang L, Rastegar S and Coté G 1999 Light backscattering polarization patterns from turbid media: Theory and experiment *Applied Optics* **38**(15), 3399–3408. doi: 10.1364/AO.38.003399.

Ramella-Roman J, Prahl S and Jacques S 2005 Three Monte Carlo programs of polarized light transport into scattering media: Part I *Optics Express* **13**(12), 4420–4438. doi: 10.1364/OPEX.13.004420.

Schäfer J 2012 'Matscat' ,`http://www.mathworks.com/matlabcentral/fileexchange/36831-matscat`.

Schäfer J and Kienle A 2008 Scattering of light by multiple dielectric cylinders: Comparison of radiative transfer and Maxwell theory *Optics Letters* **33**(20), 2413–2415. doi: 10.1364/OL.33.002413.

Schneiderheinze D H, Hillman T R and Sampson D D 2007 Modified discrete particle model of optical scattering in skin tissue accounting for multiparticle scattering *Optics Express* **15**(23), 15002–15010. doi: 10.1364/OE.15.015002.

Tishkovets V P 2008 Light scattering by closely packed clusters: shielding of particles by each other in the near field *Journal of Quantitative Spectroscopy and Radiative Transfer* **109**(16), 2665–2672. doi: 10.1016/j.jqsrt.2008.05.008.

Tuchin V, Wang L and Zimnyakov D 2006 *Optical polarization in biomedical applications* Vol. 1 Springer.

Van de Hulst H 1981 *Light scattering by small particles* Vol. 1 Dover Publications.

Voit F, Hohmann A, Schäfer J and Kienle A 2012 Multiple scattering of polarized light: comparison of Maxwell theory and radiative transfer theory *Journal of Biomedical Optics* **17**(4), 045003–1–045003–8. doi: 10.1117/1.JBO.17.4.045003.

Voit F, Schäfer J and Kienle A 2009 Light scattering by multiple spheres: Comparison between Maxwell theory and radiative-transfer-theory calculations *Optics Letters* **34**(17), 2593–2595. doi: 10.1364/OL.34.002593.

Wang X and Wang L 2002 Propagation of polarized light in birefringent turbid media: A Monte Carlo study *Journal of Biomedical Optics* **7**(3), 279–290. doi: 10.1117/1.1483315.

Xu Y 1995 Electromagnetic scattering by an aggregate of spheres *Applied Optics* **34**(21), 4573–4588. doi: 10.1364/AO.34.004573.